



An integrated description of terahertz generation through optical rectification, charge transfer, and current surge

Klaas Wynne *, John J. Carey

Department of Physics, University of Strathclyde, 107 Rottenrow, Glasgow G4 0NG, Scotland, UK

Received 11 February 2005; received in revised form 17 May 2005; accepted 24 June 2005

Abstract

Ultrafast terahertz pulses can be generated through a number of processes such as optical rectification in an electro-optic crystal, a current surge in a biased photoconductive antenna, or charge transfer in aligned molecules. It will be shown that all these rectification processes can be described by a single analytical formula in the frequency domain. A recipe is given for the quick calculation of terahertz waveforms generated through any rectification process and detected through electro-optic sampling. This theory is compared with experimentally measured terahertz waveforms. © 2005 Elsevier B.V. All rights reserved.

PACS: 42.65.-k; 42.65.Re; 78.47.+p

Keywords: Rectification; Ultrafast; Terahertz

1. Introduction

Although terahertz approximately single-cycle sub-picosecond pulses were generated for the first time a long time ago through optical rectification [1] and using photoconductive switches [2], it has been the development of efficient techniques for optical rectification [3,4] and electro-optic sam-

pling [5–10] in crystals such as ZnTe that has allowed the great expansion of research using terahertz frequency radiation [11–13]. Terahertz pulses are now used for applications as diverse as spectroscopy of liquids, solids and gasses [13], fundamental optics [14–17], studies of plasmas [18], imaging [19], and the measurement of relativistic electron bunches [20,21]. For most of these applications, the precise form of the terahertz wave generated is not that important. For example, in terahertz time-domain spectroscopy, one measures the waveform through electro-optic sampling with and without a sample in the beam

* Corresponding author. Tel.: +44 141 548 3381; fax: +44 141 552 2891.

E-mail address: klaas.wynne@phys.strath.ac.uk (K. Wynne).

and the spectrum of the sample is determined by a ratio of these two results. However, for some applications in which the terahertz waveform itself is analyzed in order to extract physical parameters, it is crucial to know exactly what is measured. There have been a few studies analyzing the electro-optic sampling signal and its dependence on pulse width, pulse wavelength, dispersion at terahertz frequencies, and dispersion in the electro-optic tensor [8,22–25], and one recent study that also includes optical rectification [26].

Optical rectification in crystals such as ZnTe, GaP, and GaSe is well understood. However, there are other methods of terahertz pulse generation that may appear to be based on entirely different physical processes. Terahertz pulse generation in biased photoconductive antennas relies on the excitation by a visible light pulse of carriers from the valence to the conduction band where they are accelerated in an external DC electric bias field. The resultant current surge then gives rise to the emission of an electromagnetic terahertz pulse [27]. In a number of recent experiments [28–32] it has been shown that microscopic currents within molecules due to intramolecular photoinduced charge transfer can give rise to the emission of terahertz radiation as well if these molecules are somehow aligned. When aligned, the microscopic currents on the individual molecules add up to produce a macroscopic current that radiates an electromagnetic field. In the latter example of terahertz pulse generation by molecular charge transfer, measurement of the time dependence of the electromagnetic transient allows one to extract information about the microscopic currents. Similar analysis of terahertz pulse shapes has been used to understand charge generation in semiconductors [33], semiconducting polymers [34], and demagnetization of ferromagnetic films [35]. In these cases, it is necessary to have a model describing the absolute terahertz pulse shape (rather than changes in the pulse shape) and how this shape is affected by linear absorption, reflections, and propagation. It is also preferable to have an analytical model in order to facilitate curve fitting to extract microscopic parameters.

The three methods of generating terahertz pulses, optical rectification, current surge, and charge transfer, are all manifestations of the same physical process: rectification. Here, it will be shown that one can derive a general expression from the Maxwell wave equation for rectification. The result is a frequency-domain equation for the generated (terahertz) electromagnetic field after propagation through a rectifying sample, which has an embedded function representing the local (microscopic) generation process. Expressions will be derived for this function for the cases of optical rectification, charge transfer, and current surge. Using simple expressions for propagation from the emitter into the far field and electro-optic sampling, the theory can then be compared with experimental data for these three cases.

2. Coherent and incoherent optical rectification

In general, a description of the generation process for terahertz radiation in a generator with a finite thickness is a complicated three-dimensional problem. Often terahertz pulses are generated in a biased photoconductive antenna based on a semiconductor such as GaAs. As the (low-power) absorption depth of GaAs at 800 nm is about 1 μm , it is typically assumed that it is reasonable to describe the generation region as infinitely thin. In the experiments described here, such an assumption is certainly not correct: The generation region is approximately equal to the sample length, which can be as much as a millimeter. Nevertheless, it may be reasonable to assume that the generation region is much shorter than the distances over which the curvature of the beam wavefront varies. In other words, the generation region is much shorter than any of the focal lengths of optical elements used in the setup. Diffraction of the terahertz beam, although it will also take place over the length of the generator or detector, can then be included separately. Under this assumption, the electromagnetic waves can be described as locally plane waves (see Fig. 1) and one may use the one-dimensional Maxwell wave equation, which, in SI units, is

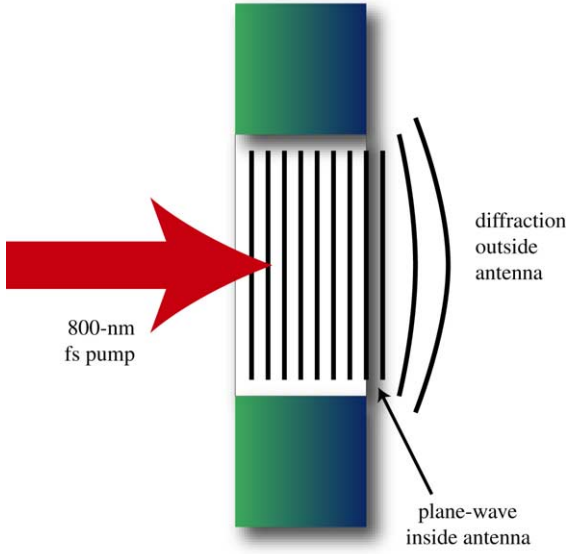


Fig. 1. The plane-wave approximation is made inside the antenna.

$$\begin{aligned} & \left[-\frac{\partial^2}{\partial z^2} + \frac{1}{c^2} \frac{\partial^2}{\partial t^2} \right] E(z, t) \\ & = -\mu_0 \frac{\partial^2}{\partial t^2} P(z, t) - \mu_0 \frac{\partial}{\partial t} j(z, t), \end{aligned} \quad (1)$$

where z is the propagation direction, E the electric field, P the local polarization, and j the local current density. From now on, the source current will be set to zero without loss of generality. The wave equation is solved in the frequency domain and the following *ansatz* is made:

$$\begin{cases} \tilde{E}(z, \omega) = A(z)\tilde{E}(\omega), \\ \tilde{P}(z, \omega) = A(z)\tilde{E}(\omega)\varepsilon_0\tilde{\varepsilon}(\omega) + \varepsilon_0\tilde{p}(z, \omega), \end{cases} \quad (2)$$

where $A(z)$ is a function describing the gain (or loss) a terahertz field experiences on traversing the sample, $\tilde{E}(\omega)$ is the spectrum of the terahertz field, $\tilde{\varepsilon}(\omega)$ is the dielectric response function of the medium, and $\tilde{p}(z, \omega)$ is a function describing the microscopic polarization induced by some external force. This *ansatz* is not equivalent to the slowly varying envelope approximation [36]. The *ansatz* for the polarization contains two terms: The first takes into account the linear optical response of the medium and the second any other

polarization such as that due to rectification. Using Laplace transformation, we find the solution

$$\begin{aligned} \tilde{E}(z, \omega) &= \tilde{E}(0, \omega) e^{i\lambda z} - \frac{k}{\tilde{n}(\omega)} \int_0^z d\zeta \tilde{p}(\zeta, \omega) \\ &\quad \times \sin(\lambda(z - \zeta)). \end{aligned} \quad (3)$$

In this expression, the first term describes the absorption of any external terahertz field inside the medium, where $\lambda = k(1 + \tilde{\varepsilon}(\omega))^{1/2} \equiv k\tilde{n}(\omega)$ is the complex wavevector inside the crystal. The free-space wavevector of the terahertz field is $k = \omega/c$, and the frequency-dependent complex refractive index is $\tilde{n}(\omega)$, which can be related through $\tilde{n}(\omega) = n + i\alpha/(2k)$ to the (real-valued) refractive index n and the power absorption coefficient α .

Now it is important to make a reasonable assumption as to the form of the “other” polarization while maintaining generality. In all cases of relevance, a (visible) excitation laser pulse travels through the medium inducing a polarization oscillating at terahertz frequencies. The most general requirement then is that the medium responds causally and begins somewhere in space, which might as well be taken to be $z = 0$, leading to

$$\tilde{p}(z, \omega) = \tilde{f}(\omega) e^{ik_{\text{VIS}}z} \theta(z), \quad (4)$$

where $\tilde{f}(\omega)$ is the frequency-domain representation of the response of the medium, $\theta(z)$ is the Heaviside step function, and n_{VIS} is the group index of the excitation pulse determining its group velocity through $v_{\text{group}} = c/n_{\text{VIS}}$. Using Eq. (4) for the polarization in Eq. (3) results in the analytical solution

$$\begin{aligned} \tilde{E}(z, \omega) &= \tilde{E}(0, \omega) e^{ik\tilde{n}z} - \frac{\tilde{f}}{2\tilde{n}} \left[\frac{e^{ikz(\tilde{n} - n_{\text{VIS}})} - 1}{n_{\text{VIS}} - \tilde{n}} \right. \\ &\quad \left. + \frac{1 - e^{-ikz(\tilde{n} + n_{\text{VIS}})}}{n_{\text{VIS}} + \tilde{n}} \right] e^{ik_{\text{VIS}}z}. \end{aligned} \quad (5)$$

The second term between brackets in the above equation corresponds to a backwards propagating wave and can be ignored in what follows. The first term between brackets is the resonant generation term and is of a more general form than a previously published expression [26].

In Section 3, models for the medium response $\tilde{f}(\omega)$ will be discussed. Fig. 2 shows the predicted

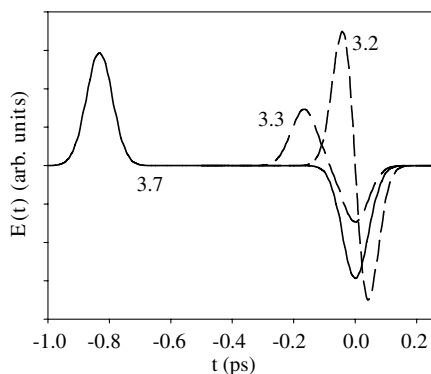


Fig. 2. Generation of terahertz pulses through rectification. The terahertz phase index has been set to $\tilde{n} = 3.2$ and the three curves correspond to a visible excitation-pulse group index of $n_{\text{VIS}} = 3.7, 3.3,$ and 3.2 . The curve for $n_{\text{VIS}} = 3.7$ has been multiplied by a factor of 10 for clarity. The zero of time has been defined as the time when the visible excitation pulse exits the generation medium.

terahertz pulse shapes for an instantaneously responding sample calculated from Eq. (5) by a numerical Fourier transform to the time domain. In calculating these curves, it has been assumed that the refractive (phase) index in the far-infrared region is constant. When the terahertz phase index is very different from the visible group index ($\tilde{n} = 3.2$ and $n_{\text{VIS}} = 3.7$), Eq. (5) predicts the generation of a pair of terahertz pulses: one traveling with the terahertz phase velocity and one with the group velocity of the visible pulse. In this case (and in the near field!), the two terahertz pulses are a faithful copy of the envelope of the excitation pulse although with opposite sign. When the phase and group index are closer in value, the generation of terahertz radiation is more efficient and the output is a single terahertz pulse, which, in the limit $\tilde{n} = n_{\text{VIS}}$, is shaped as the derivative of the visible pulse envelope.

3. Models for the source of the terahertz polarization

In Section 2, it was assumed that the polarization induced in the medium by the visible pump pulse can be written as

$$\tilde{P}(z, \omega) = \varepsilon_0 \tilde{f}(\omega) e^{ik_{\text{VIS}}z} \theta(z). \quad (6)$$

In the following, expressions will be derived for $\tilde{f}(\omega)$ for various appropriate models.

3.1. Optical rectification

Optical rectification is best understood in the frequency domain as a difference-frequency mixing process. Thus, the local microscopic second-order polarization at frequency ω is given by [36]

$$P(\omega) = \varepsilon_0 \chi^{(2)}(\omega; \Omega, \Omega - \omega) E(\omega) E^*(\Omega - \omega), \quad (7)$$

which oscillates at the difference frequency. Ultrashort pulses have a distribution of frequencies and therefore the above expression has to be integrated over the distribution of Ω s. It then follows that for optical rectification one can set the medium response to

$$\tilde{f}(\omega) = \chi^{(2)}(\omega) \tilde{I}_{\text{pump}}(\omega), \quad (8)$$

where $\tilde{I}_{\text{pump}}(\omega)$ is the *Fourier transform of the intensity envelope* of the pulse rather than the spectrum of the laser pulse. Thus, if only a single pulse is rectified, the optical rectification signal is not sensitive to chirp in the visible pulse for a given intensity envelope duration. Chirp may have an effect when a pair of visible pulses is rectified [37].

3.2. Terahertz emission due to charge transfer

When a molecule is electronically excited or changes from one electronic state to another, it often changes its permanent dipole moment through an intramolecular charge-transfer process [38]. It has been shown that if these molecules are aligned to some degree, this will lead to the emission of electromagnetic radiation. The molecules can be aligned by being confined in a crystal lattice [28,29], by an external DC electric field [30], or by oriented deposition on a surface [31,32]. The source of alignment is not relevant here since the degree of alignment is not expected to change on the time scale of a typical terahertz pulse (~ 1 ps).

First, a model has to be defined describing how exciting a particular molecule with an ultrashort excitation pulse will change the permanent dipole moment within the molecule itself. Two models will be considered. First (see Fig. 3), a molecule

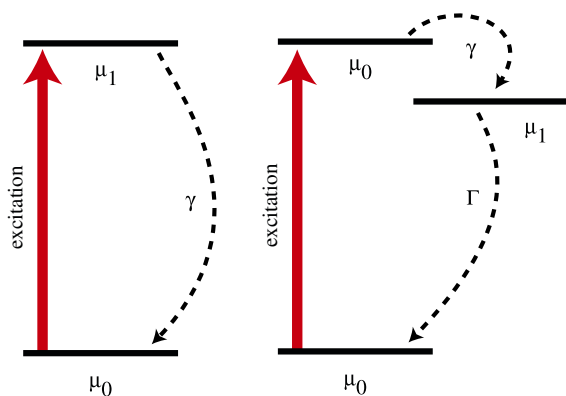


Fig. 3. Two charge-transfer models considered in the text. (left) Direct charge transfer. (right) Indirect charge transfer with one intermediate state.

undergoing direct charge transfer [38], i.e., excitation causing an instant change in dipole moment $\Delta\mu$ followed by a slower return with rate γ to the original dipole moment. Second, a molecule undergoing indirect charge transfer in which excitation is followed by a change of the dipole moment with rate γ followed by a return to the original state with rate Γ . In experiments measuring terahertz radiation from charge transfer, the field is typically measured in the far field (except for one report [31]) and therefore one only has to consider the *change* in dipole moment. Thus, the time-dependence of the permanent dipole moment in the case of direct charge transfer is

$$\Delta\mu(t) = I_{\text{pump}}(t) \otimes [\theta(t)\Delta\mu e^{-\gamma t}], \quad (9)$$

where “ \otimes ” indicates a convolution, $\Delta\mu$ is the change in permanent dipole moment and $\theta(t)$ is the Heaviside step function ensuring the expression is causal. In the case of indirect charge transfer it is

$$\Delta\mu(t) = I_{\text{pump}}(t) \otimes [\theta(t)\Delta\mu (e^{-\Gamma t} - e^{-\gamma t})]. \quad (10)$$

The above descriptions of the change of the permanent dipole moment only consider changes in magnitude. In general, one would have to consider changes in direction as well.

If the molecule undergoing photoinduced charge transfer is embedded in a dielectric such as a liquid, crystal or protein matrix, the surrounding medium will respond to the electrostatic

changes taking place in the molecule. Here, a solute is considered with a charge distribution that can be approximated as a point dipole μ . The Onsager cavity model [39] has this dipole sitting in an empty (spherical) cavity surrounded by a continuous dielectric with dielectric constant ϵ . It will be assumed [40] that electrostatics can be used if the Onsager cavity problem is solved in the frequency domain. This ignores retardation effects, which will be minimal over molecular distances in any case. Fourier transformation can be used at the end to return to a time-domain picture. Solving the Onsager cavity problem by matching the scalar potential inside and outside the cavity leads to the well-know reaction field inside the cavity [39]. Outside the cavity, the dipole moment plus the dielectric response appears like an enhanced dipole moment given by the expression

$$\vec{\mu}_{\text{R}} = \frac{3\epsilon}{2\epsilon + 1} \vec{\mu}. \quad (11)$$

It will be assumed [40] that the above equation can be considered valid for all frequencies and therefore that the time-dependent effective dipole moment is simply its Fourier transform. The macroscopic polarization of the sample is then given by

$$\tilde{P}(\omega) = N \frac{3\tilde{\epsilon}(\omega)}{2\tilde{\epsilon}(\omega) + 1} \tilde{\mu}(\omega), \quad (12)$$

where N is the number density of excited molecules and $\tilde{\mu}(\omega)$ is the Fourier transform of the appropriate function describing the time dependence of the molecular dipole moment. Using the Fourier transform of Eq. (9) or Eq. (10), one can finally derive the sample response function. In the case of *direct charge transfer*,

$$\tilde{f}(\omega) \equiv \frac{3\tilde{\epsilon}(\omega)}{2\tilde{\epsilon}(\omega) + 1} \frac{N\Delta\mu\epsilon_0^{-1}}{\gamma - i\omega} \tilde{I}_{\text{pump}}(\omega) \quad (13)$$

is found and in the case of *indirect charge transfer*,

$$\tilde{f}(\omega) \equiv \frac{3\tilde{\epsilon}(\omega)}{2\tilde{\epsilon}(\omega) + 1} \frac{N\Delta\mu}{\epsilon_0} \left(\frac{1}{\Gamma - i\omega} - \frac{1}{\gamma - i\omega} \right) \tilde{I}_{\text{pump}}(\omega) \quad (14)$$

is found. The effect of the dielectric response function in Eq. (12) is to introduce a delay in the response: Even an instantaneous change of the

molecular dipole moment will be observed at some distance away as a fractional instantaneous change proportional to the infinite-frequency dielectric constant and a slow response whose precise form and magnitude depends on the solvent dynamics.

3.3. Terahertz emission due to carrier acceleration

A third fundamental case is that of carrier acceleration in an external DC electric field. This situation occurs in biased-semiconductor or conducting-polymer [34] antennas commonly used for terahertz generation. In such a device, a pump laser pulse excites carriers from the valence to the conduction band. In the conduction band, the carriers are essentially a free plasma, which can be described with the Drude model, i.e., the velocity of the carriers is governed by the differential equation [41]

$$\frac{dv}{dt} = -\gamma_s v + \frac{e}{m^*} E, \quad (15)$$

where γ_s is the momentum relaxation rate, m^* the effective mass of the carriers, and E is the DC bias field (in general the external DC bias field plus the terahertz field generated elsewhere in the sample). When an electron separates from a hole, a dipole is formed with magnitude $\mu = -ex$, where x is their separation. Using the Drude equation (15), it follows:

$$P(t) = I_{\text{pump}}(t) \otimes \frac{-e^2 E n_f}{\gamma_s m^*} \theta(t) \int_0^t d\tau [1 - e^{-\gamma_s \tau}], \quad (16)$$

where P is the polarization density, and n_f the carrier density. These expressions do not include the effect of carrier recombination or trapping, which will usually have an effect on a much longer time-scale than is of interest here. The effects of saturation (for example, the generated terahertz field canceling part of the DC bias field) are also not included in the interests of simplicity. However, carrier recombination can easily be accommodated by replacing the integrand in Eq. (16) by $\exp(-\Gamma\tau) - \exp(-\gamma_s\tau)$, where Γ is the carrier recombination rate (and $\Gamma \ll \gamma$).

By taking the Fourier transform of Eq. (16) and adding in the dielectric response of the surrounding medium as in Eq. (12) in the previous subsection, the response function for the current-surge model is found

$$\tilde{f}(\omega) \equiv \frac{3\tilde{\epsilon}(\omega)}{2\tilde{\epsilon}(\omega) + 1} \frac{1}{\epsilon_0} \frac{-e^2 E n_f}{\gamma_s m^*} \times \frac{1}{-i\omega} \left(\frac{1}{\Gamma - i\omega} - \frac{1}{\gamma_s - i\omega} \right) \tilde{I}_{\text{pump}}(\omega). \quad (17)$$

The factor $(-i\omega)^{-1}$ in the above expression is a result of the integral in Eq. (16). It is the principal reason why terahertz pulses from biased photoconductive antennas have a single-cycle or even half-cycle appearance.

4. Propagation into the far field

In most terahertz experiments, the field is measured in the far field. A typical setup may consist of a generator, a collimating mirror, a certain propagation distance, a focusing mirror, and finally a detector. A typical f -number of the collimating optic of about 3 implies that the far field is typically already reached after the first mirror. The effect of propagation into the far field on the pulse shape or its spectrum can be calculated using Huyghens–Fresnel diffraction theory [42]. In the time domain, the field in the far field can be related to that in the near field by a temporal derivative (as well as a reduction of the field amplitude inversely proportional to distance). In our experiments [28,43], the visible excitation pulse is focused through the generation medium and onto the electro-optic sampling detection crystal. In this case, the far field is again characterized by a temporal derivative (and a logarithmic decay of the amplitude with focal distance). In the frequency domain, the time derivative corresponds with a multiplication by $-i\omega$.

5. Electro-optic sampling

The terahertz field is typically measured using electro-optic sampling. Phasematching equations

for electro-optic sampling have already been presented in the literature [7,8,23,25]. In electro-optic sampling, a (visible) gate pulse travels along with a terahertz pulse in an electro-optic crystal. The signal consists of elliptical polarization impressed onto the gate beam by the Pockels effect induced by the terahertz field and detected by balanced detection. The electro-optic sampling signal in this case is given by

$$\begin{aligned} \Delta I_{\text{EOS}}(\tau) \\ \propto r_{41} \int_0^L dz \int_{-\infty}^{\infty} dt I_{\text{gate}}(t - \tau - zn_{\text{VIS}}/c) E_{\text{THz}}(z, t), \end{aligned} \quad (18)$$

where τ is the relative delay of the gate pulse and L the length of the electro-optic detection crystal. By writing the terahertz field as a Fourier transform, this expression can be rewritten as

$$\begin{aligned} \Delta I_{\text{EOS}}(\tau) \propto r_{41} \int d\omega e^{-i\omega\tau} \tilde{I}_{\text{gate}}(\omega) \tilde{E}_{\text{THz}}(0, \omega) \\ \times \frac{e^{i\omega[\tilde{n} - n_{\text{VIS}}]L/c} - 1}{i\omega[\tilde{n} - n_{\text{VIS}}]/c}, \end{aligned} \quad (19)$$

where $\tilde{E}(0, \omega)$ is the Fourier transform of the terahertz pulse at the entrance of the electro-optic detection crystal. Unfortunately, the electro-optic sampling signal is not directly proportional to the terahertz field but incorporates a phasematching term. Only when the gate pulse is a delta function and the detection crystal infinitely thin, is the detected signal linearly proportional to the terahertz-pulse electric field. Modifications can be made to incorporate the effects of dispersion in the electro-optic coefficient r_{41} and frequency-dependent reflection of the terahertz wave on entering the electro-optic crystal [24,25]. This expression for the electro-optic-sampling signal strength is not the same as our expression for terahertz generation equation (5). The reason is that in electro-optic sampling, the field that is modified and detected (by a square-law detector) is a visible femtosecond probe laser pulse. For this visible pulse, it is very reasonable to make the slowly varying envelope approximation [36] unlike for the terahertz pulse.

6. Recipe

Based on the equations given in the previous sections, one can now define a recipe for calculating the measured signal in an experiment in which a terahertz pulse is generated through rectification and detected (in the far field) by electro-optic sampling. The generated field is

$$\tilde{E}_{\text{THz,NF}}(z, \omega) = -\frac{\tilde{f}}{2\tilde{n}} \frac{e^{ikz(\tilde{n} - n_{\text{VIS}})} - 1}{n_{\text{VIS}} - \tilde{n}} e^{ikn_{\text{VIS}}z} \quad (20)$$

in the near field, where one has to choose the right form for $\tilde{f}(\omega)$. In the far field, this becomes

$$\tilde{E}_{\text{THz}}(z, \omega) = -i\omega \tilde{E}_{\text{THz,NF}}(z, \omega). \quad (21)$$

Finally, Eq. (19) is used to calculate the electro-optic sampling signal. The response function $\tilde{f}(\omega)$ is given by Eq. (8) for *optical rectification*, Eq. (13) for *direct charge transfer*, Eq. (14) for *indirect charge transfer*, and Eq. (17) for the *current-surge model*. In all cases, the response function is of the form

$$\tilde{f}(\omega) = \tilde{r}(\omega) \tilde{I}_{\text{pump}}(\omega), \quad (22)$$

where $\tilde{r}(\omega)$ is a property of the medium only. Thus, the signal can be written as

$$\begin{aligned} \Delta I_{\text{EOS}}(\tau) \propto \int d\omega e^{-i\omega\tau} \tilde{I}_{\text{pump}}(\omega) \tilde{I}_{\text{gate}}(\omega) \\ \times [i\omega] \tilde{\zeta}_{\text{gen}}(\omega) \tilde{r}(\omega) \tilde{\zeta}_{\text{det}}(\omega), \\ \tilde{\zeta}_{\text{gen}}(\omega) \equiv \frac{e^{ikL_1(\tilde{n} - n_{\text{VIS}})} - 1}{2\tilde{n}(n_{\text{VIS}} - \tilde{n})}, \\ \tilde{\zeta}_{\text{det}}(\omega) \equiv \frac{e^{ikL_2[\tilde{n} - n_{\text{VIS}}]} - 1}{ik[\tilde{n} - n_{\text{VIS}}]}, \end{aligned} \quad (23)$$

where L_1 is the length of the generation medium and L_2 that of the detection crystal. The function $\tilde{\zeta}_{\text{gen}}$ is seen to be the generation phasematching condition and $\tilde{\zeta}_{\text{det}}$ that of the detection. A factor $\exp(ikn_{\text{VIS}}L_1)$ has been dropped from the generation phasematching function (cf. Eq. (20)) in order that time zero is defined as the time when the excitation pulse exits the generation medium. However, when the generation medium attenuates the pump beam, it is critical to put back in a factor $\exp(-k\text{Im}[n_{\text{VIS}}]L_1)$ with $\text{Im}[n_{\text{VIS}}]$ representing the

attenuation. The term $[i\omega]$ in Eq. (23) may be dropped to obtain a near-field result (for example, when the detection crystal is on top of the generation medium [31]) although the above expression does not contain any DC components that might be present in that case. Extra terms can be added to Eq. (23) to account for Fresnel reflections or propagation through humid air. The whole calculation of the signal is analytical except for the final Fourier transform, which will have to be calculated numerically. Any pulse shape can be used for the pump and gate pulses although in practice it is convenient to use a Gaussian

$$\tilde{I}_{\text{pump/gate}}(\omega) \propto \exp(-\omega^2 \text{FWHM}^2 / (16 \ln 2)) \quad (24)$$

or a sech-squared pulse

$$\tilde{I}_{\text{pump/gate}}(\omega) \propto \omega \text{csch}(\text{FWHM} \pi \omega / (4 \text{arcsinh } 1)), \quad (25)$$

where FWHM is the full-width at half maximum of the intensity envelope in the time domain.

In order to calculate the signal, one requires the far-infrared phase index $\tilde{n}(\omega)$ over the relevant frequency range and the group index at the wavelength of the pump/gate pulse for both the generation and detection medium. The appendix provides these data for the crystal ZnTe, the liquid chloroform, and for Infrasil glass.

7. Practical examples

In the following, some examples will be given of the application of the recipe to a number of practical cases. The experimental setup used in these experiments has been described previously [28]. Briefly, the laser system uses 40–80-fs 800-nm 1–2-mJ pulses with a 1-kHz repetition rate. The largest fraction of the beam ($\sim 95\%$) is focused through the samples in order to produce pre-focused terahertz radiation. The terahertz pulses are detected using electro-optic sampling with the remaining 5% of the laser beam in 0.5- or 0.2-mm thickness $\langle 110 \rangle$ -cut ZnTe crystals. The transmitted gate beam is analyzed with a quarter-wave plate and a Glan–Thompson polarizer and detected by two balanced Si PIN photodiodes.

7.1. Rectification and electro-optic sampling in ZnTe

The first case analyzed is that of standard optical rectification in ZnTe. The ZnTe crystals used in this study have been obtained from Ingcryst Laser Systems and were cut along the $\langle 110 \rangle$ plane. Both normal and high-resistivity crystals have been used but no difference was noticeable in these studies. The far-infrared absorption spectrum of these crystals has been measured and these data analyzed to get an accurate formula for the dispersion of the dielectric function (see the appendix).

Fig. 4 shows the measured terahertz pulse generated in a 0.5-mm ZnTe crystal and detected in a 0.2-mm ZnTe crystal. The theoretical curve in Fig. 4 has been generated from the recipe Eq. (23) with an instantaneous crystal response ($\tilde{r}(\omega) = 1$), and 60-fs FWHM sech^2 pump and gate pulses. Non-linear least-squares curve fitting has been used to optimize the amplitude and zero of time, which are essentially arbitrary in this experiment. Curve fitting has also been used to optimize the value of the group index experienced by the pump and gate pulses. It was found that the precise center wavelength of the laser could vary slightly from day to day, justifying this approach. The group index used for Fig. 4 is $n_{\text{VIS}} = 3.13$ which is close to a value of $n_{\text{VIS}} = 3.28$ for the

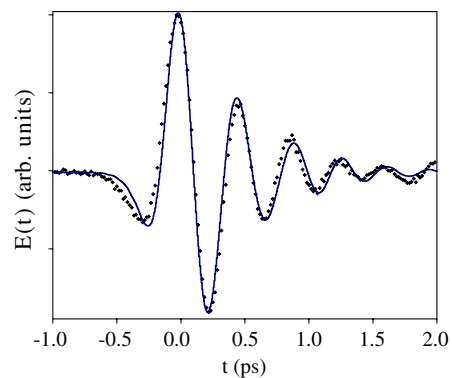


Fig. 4. Terahertz pulse generated in a 0.5-mm and detected in a 0.2-mm $\langle 110 \rangle$ -cut ZnTe crystal with an 800-nm 40-fs pulse. The curve is a theoretical fit with $n_{\text{VIS}} = 3.13$ and sech^2 pump and gate pulses with FWHM = 60 fs. Amplitude, zero delay, and group index were left as free fit parameters.

group index at 800 nm in ZnTe calculated from refractive index data [44].

It can be seen that the correspondence between experiment and theory is quite good in the case of optical rectification in ZnTe. The far-infrared refractive index of ZnTe varies from about 3.1 at low frequencies to about 4 at 5 THz. The frequency at which the terahertz phase index equals the visible (nominally 800 nm) group index, determines the dominant frequency of the produced terahertz pulse itself, which is about 2 THz in our case. Any terahertz radiation generated below this frequency will propagate faster than the visible pump pulse. This explains the signal at negative delay and the overall chirped appearance of the terahertz pulse. The correspondence between experiment and theory is poorest at negative delay indicating a problem at low frequencies. This could be due to errors in the dispersion curve or, more likely, the fact that diffraction during generation has not been included in the theory.

7.2. Terahertz emission by charge transfer in solution

The second case considered here is that of terahertz generation through charge transfer in solution. Fig. 5 shows a terahertz pulse emitted by a sample consisting of a solution of Reichardt's dye in chloroform polarized by an external electric field.

The detection of the terahertz radiation is through standard electro-optic sampling in a 0.5-mm $\langle 110 \rangle$ ZnTe crystal as in the previous section. The sample consists of a 1-mm thickness 1-cm width Infrasil glass cuvette filled with a solution of Reichardt's dye (betaine) in chloroform. All chemicals were obtained from Sigma–Aldrich and used without further purification. Two 0.5-mm diameter copper-wire electrodes were inserted into the solution with a separation of 8 mm in order to apply a polarizing electric bias field. The bias field was a 12 kV/cm quasi-DC (100-ns pulse width) electric field pulsing synchronously with the 1-kHz repetition rate laser.

When Reichardt's dye is excited at 800 nm, the molecule instantly changes its dipole moment. This is followed by a thermally induced electron-transfer reaction returning the system back to its ground state. The rate of back electron transfer is strongly controlled by the solvent [45,46] and takes place in about 2.8 ps in chloroform [46,47]. Fig. 5 also shows a theoretical calculation based on the recipe equation (23) using Eq. (13) to model the direct electron-transfer response of Reichardt's dye. Also included were Fresnel reflections off the solution-glass and glass-air interfaces as well as absorption in the glass wall of the cuvette. The

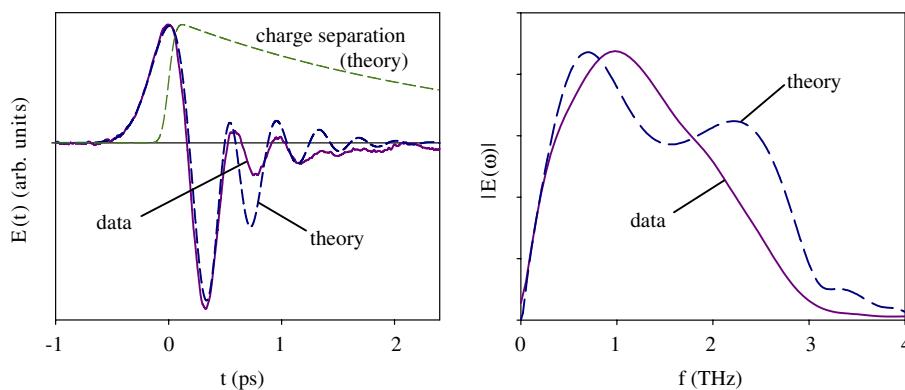


Fig. 5. Terahertz emission due to photoinduced electron transfer in Reichardt's dye in chloroform and comparison with theory. The figure on the left shows the time-domain data and a comparison with theory as well as a curve indicating the time scale of thermal back electron transfer in Reichardt's dye. The figure on the right shows the Fourier transforms of the data and theory. In calculating the theoretical curve, 80-fs FWHM Gaussian pulses were used for the pump and gate pulses, a group index in chloroform of $n_{VIS} = 1.45461$, and 1% transmission of the pump pulse through the sample. Parameters for detection are the same as in Fig. 4.

dispersion of the far-infrared absorption and refractive index of chloroform and Infrasil glass are discussed in the appendix. The theoretical curve in Fig. 5 has no free fit parameters except zero delay and overall amplitude, and the electron-transfer time was set at 2.8 ps. The group index in chloroform at 800 nm was calculated from dispersion data as $n_{\text{VIS}} = 1.45461$. Transmission of the pump pulse through the sample was set at 1%.

The correspondence between theory and data in Fig. 5 is not great although the overall appearance is similar. It was found that the precise shape of the theoretical curve depends strongly on the far-infrared properties of the materials involved, i.e., chloroform and the glass of the cuvette used. In addition, these properties are changeable; for example, chloroform is slightly hygroscopic and a small amount of water can greatly increase the far-infrared absorption. The shape of the theoretical curve is not very sensitive to the rate of thermal back electron transfer: varying the electron-transfer time between 0.28 and 28 ps has a noticeable but minor effect on the calculated curve.

7.3. Terahertz emission by large-area biased photoconductive antennas

The third and final case considered here is terahertz emission from a large-area biased photoconductive antenna. This antenna consists of a

450- μm thickness semi-insulating $\langle 1\ 0\ 0 \rangle$ -cut GaAs wafer with silver-paint electrodes on either side with a separation of 5 mm. A pseudo DC bias voltage was applied to the antenna as described in the previous subsection with a field strength of 4 kV/cm. The optical setup was also as described above with the excitation beam focused through the sample and electro-optic sampling in a 0.5-mm $\langle 1\ 1\ 0 \rangle$ -cut ZnTe crystal and balanced detection.

Fig. 6 shows the terahertz pulse measured experimentally in this setup and a theoretical curve calculated using the recipe of Eq. (23) and the response function equation (17) to model the current surge. The detection through electro-optic sampling was modeled as described above with the dispersion data from Appendix. The far-infrared dielectric properties of GaAs have been modeled with an oscillator equation (Eq. (26)) fit to published absorption and refractive-index data [44]. The refractive index dispersion around 800 nm has been modeled with a 3rd-order polynomial from which a group index at 800 nm of $n_{\text{VIS}} = 4.2039$ was derived. An assigned imaginary part of the 800-nm refractive index has been used to incorporate attenuation as described above. For the current-surge model Eq. (17) a scattering time of 100 fs and a recombination time of 0.5 ns have been used. In the calculation, it has been assumed that the 800-nm generation pulse is absorbed by GaAs in a 1- μm thick layer to 1%

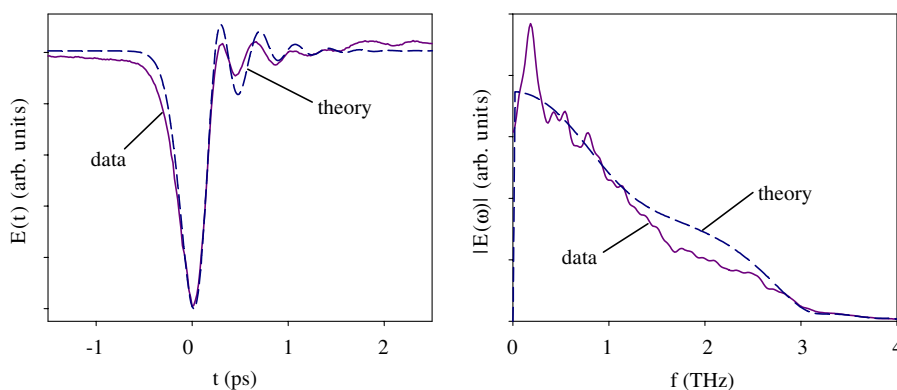


Fig. 6. Terahertz pulse generated in a DC-biased GaAs large-area photoconductive antenna and detected in a 0.5-mm ZnTe crystal through electro-optic sampling. The parameters for the theoretical curve are: 80-fs FWHM Gaussian excitation and gate pulses, generation in 1- μm GaAs with 1% transmission through this layer, propagation through 440- μm unexcited GaAs, current-surge model with $\tau_{\text{scattering}} = 100$ fs, $\tau_{\text{recombination}} = 0.5$ ns.

of its original strength after which the generated terahertz pulse propagates through the remaining 449 μm of unexcited GaAs. In practice, the exact thickness of the excited layer has very little if any influence on the terahertz pulse shape. Considering the simplicity of the model, the agreement between data and theory in Fig. 6 is excellent.

8. Conclusion

The recipe presented here allows quick and nearly analytical calculation of terahertz pulse shapes generated through rectification and detected (in the near or far field) through electro-optic sampling. The calculation is straightforward enough that it can be incorporated into curve-fitting programs and used to extract useful parameters from the data. Terahertz pulse generation has been modeled before using purely numerical methods such as the finite difference time-domain (FDTD) technique [48]. Such purely numerical techniques are required to describe pump-probe type experiments but are overkill for (essentially) linear-optics experiments as described here. We have set up our own one-dimensional FDTD program and checked that the nearly analytical calculations presented here give identical results.

In the three experimental cases described here, the correspondence between theory and experiment is good although deviations on the order of 5–10% do occur. There are a number of possible causes for these deviations. First of all, one needs an accurate description of the dispersion in the dielectric properties of the materials involved. Especially in the charge-transfer experiments, this is crucial as the solvents used have strong absorption and dispersion in the far infrared magnifying the potential problems. In addition, the material of the cell holding the sample may be strongly dispersive.

Dispersion at the visible wavelengths of the pump and gate lasers has not been included at all here. In fact, ZnTe introduces a large group-velocity dispersion that will broaden the visible pulse on propagation through the crystal. Based on the dispersion of ZnTe around 800 nm [44] one calculates a GVD of 1.7 ps^2/m , which would broaden a 40 fs pulse to 72 fs in a 0.5-mm ZnTe

crystal. To accommodate the effects of pulse broadening, we have simply used slightly longer pulse widths in the theory than those measured experimentally (i.e., 60–80 fs for an experimental pulse width of about 40 fs). It is possible to incorporate the effects of GVD for Gaussian pulses in the recipe at the expense of a much more complicated expression. It has also been seen in preliminary experiments (data not shown) that the shapes of terahertz pulses generated through optical rectification in ZnTe are sensitive to the power density. This could possibly be caused by self-phase modulation and non-linear pulse broadening. The data shown here has all been collected at powers low enough to avoid such non-linear effects.

The calculation of the terahertz pulse shape generated in a large-area biased photoconductive antenna is somewhat suspicious considering the approximations made. Excitation of carriers to the conduction band at the power densities used in our experiments (and most other experiments of this kind) should significantly change the dielectric properties of the substrate GaAs. The photo-generated plasma has a plasma frequency in the terahertz range resulting in enormous changes in the far-infrared refractive index and absorptivity. Moreover, saturation can lead to hole burning in the valence-band-conduction-band transition and result in changes to the group index. A precise and detailed description of these phenomena is well outside the scope of this paper.

It was concluded from the terahertz emission from electron-transfer experiment in Reichardt's dye that the signal hardly depends on the thermal back electron-transfer rate. This is not actually so surprising. From the equation describing terahertz generation, Eq. (5), and Fig. 2 it can be seen that, if the far-infrared phase index and the visible group index are approximately matched, the resulting terahertz pulse in the near field is the derivative of the local polarization. Propagation into the far field introduces an additional derivative. The local microscopic polarization in photo-excited Reichardt's dye rises with the pump pulse (~ 40 fs) and exponentially decays along with back electron transfer (~ 2800 fs in chloroform). The derivative of the rise will therefore be about 70 times greater than the derivative of the decay.

Propagation into the far field introduces another derivative and thus another factor of 70. Therefore, in the case of direct charge transfer, the vast majority of the signal will appear to have the shape of the first derivative of the pump pulse. However, with indirect charge transfer and/or by performing the experiment in the near field, it should be possible to use this technique to determine charge transfer rates directly without using spectroscopic assumptions.

Finally, the equations presented here do not take into account reflections. In high refractive-index materials such as ZnTe, a good portion of the visible and terahertz fields may be reflected off the crystal-air boundary. This results in the well-known reflection pulse some tens of picoseconds after the main pulse (in a typical ~ 1 -mm ZnTe crystal). However, it can also lead to electro-optic interaction between a visible and a terahertz pulse propagating in opposite direction. For long pulses, this may lead to further distortions in the pulse shapes.

Acknowledgements

We gratefully acknowledge financial support from the Engineering and Physical Sciences Research Council (EPSRC). We also gratefully acknowledge experimental help from and discussions with S. Jamison, D.A.J. Jaroszynski, and D. Jones at the Strathclyde Electron and Terahertz to Optical Pulse Source (TOPS) [49] and discussions with David Turton.

Appendix. Absorption and dispersion of ZnTe and chloroform in the far infrared

Infrared spectra have been taken with a Bruker Vertex 70 Fourier-transform Infrared spectrometer (FTIR) equipped with either a mid- or far-infrared-sensitive deuterated triglycine (DTGS) detectors used at room temperature. For far-infrared measurements, a multilayer Mylar beamsplitter has been used allowing the measurement of spectra from >10 to 670 cm^{-1} . The FTIR absorption spectra have been used “as is” and the effects of attenuation due to reflections at the surfaces

have been incorporated in the curve-fitting procedures. The data have been fitted using a nonlinear least-squares curve-fitting program. The uncertainties in the fit parameters are 68.3% joint-confidence intervals [50] and, therefore, take into account uncertainties resulting from correlations between the parameters.

The far-infrared absorption spectrum up to 15 THz of a 0.5-mm $\langle 110 \rangle$ ZnTe crystal is shown in Fig. 7 together with refractive index data up to 4.5 THz taken with the terahertz time-domain spectroscopy technique and extracted from previous publications [51,52]. The FTIR spectrometer used to obtain these data saturated at an optical density of 3.5–4 and therefore the strong TO-phonon band at ~ 5.5 THz could not be measured in its entirety. The spectrum is consistent with previously published results [53] above 5.8 THz. The data were curve-fitted using the dielectric function

$$\varepsilon_{\text{rel}}(\omega) = \varepsilon_s + \sum_j \frac{A_j \omega_j^2}{\omega_j^2 - \omega^2 - 2i\gamma_j \omega}, \quad (26)$$

which was used to calculate the refractive index and the apparent absorption coefficient (that is, including the effects of reflections off the front and back surface of the crystal). As no data could be obtained between 4.8 and 6.8 THz, refractive-index data [51,52] were required to get a meaningful fit below the main TO-phonon band. The fit

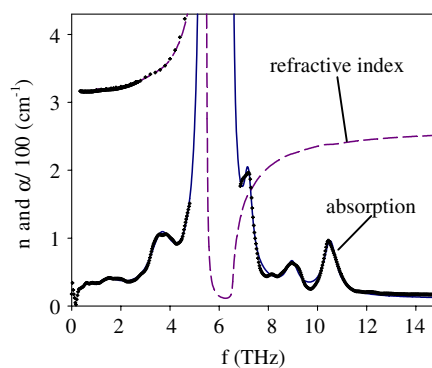


Fig. 7. Infrared absorption spectrum of a 0.5-mm ZnTe crystal. The data were taken with a Fourier-transform infrared spectrometer equipped with deuterated triglycine (DTGS) detectors for the far- and mid-infrared regions. Data up to 20 THz were taken into consideration for curve fitting. Also shown is the refractive index data up to 4.5 THz [51,52].

Table 1
Fit parameters for the infrared absorption spectrum of ZnTe

j	A_j	$\omega_j/2\pi$ (THz)	$\gamma_j/2\pi$ (THz)
1	0.3 ± 0.2	1.4 ± 0.2	0.8 ± 0.4
2	0.11 ± 0.02	3.66 ± 0.04	0.57 ± 0.09
3	3.0 ± 0.2	5.45 ± 0.05	0.028 ± 0.005
4	0.008 ± 0.002	7.18 ± 0.02	0.20 ± 0.04
5	0.0029 ± 0.0006	8.97 ± 0.05	0.28 ± 0.08
6	0.005 ± 0.0005	10.52 ± 0.03	0.31 ± 0.04

$$\varepsilon_S = 6.8 \pm 0.3.$$

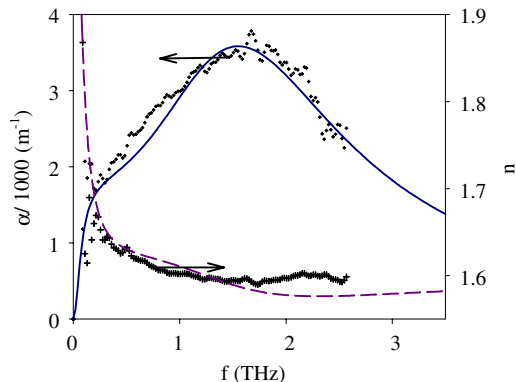


Fig. 8. Far-infrared absorption and refractive index spectrum of chloroform taken using a terahertz time-domain spectroscopy setup.

parameters are listed in Table 1. The first two bands at 1.4 and 3.66 THz are observed with equal amplitude in all the samples consistent with an assignment [54] as the TO-LA and LO-TA difference bands, respectively. The third band at 5.45 THz is the strongly infrared-active fundamental TO-phonon band [51–54], which is largely responsible for the refractive-index dispersion in this frequency region. The bands above 5.5 THz are combination bands [53]. For the simulations of terahertz pulses, only the three lowest frequency bands have been taken into consideration.

Table 2
Parameters for the infrared absorption spectrum of chloroform

j	A_j	$\omega_j/2\pi$ (THz)	$\gamma_j/2\pi$ (THz)
1	2.14	0.32	0.84
2	0.16	1.66	1.1

$$\varepsilon_S = 2.546.$$

Table 3
Parameters for the infrared absorption spectrum of Infrasil glass

j	A_j	$\omega_j/2\pi$ (THz)	$\gamma_j/2\pi$ (THz)
1	2.764	20	1.349

$$\varepsilon_S = 1.$$

Fig. 8 shows the far-infrared absorption and refractive index spectrum of chloroform. These data have been fitted to Eq. (26) with two components. The fit parameters are shown in Table 2. Chloroform is slightly hygroscopic and absorption due to trace amounts of water cannot be excluded. The peak absorption seems to be a bit high compared with published spectra [55]. Similarly, the far-infrared absorption and refractive-index spectrum of Infrasil glass was taken. These data have been fitted to a one component model with parameters as shown in Table 3.

References

- [1] D.H. Auston, K.P. Cheung, J.A. Valdmanis, et al., Phys. Rev. Lett. 53 (1984) 1555.
- [2] D.H. Auston, K.P. Cheung, P.R. Smith, Appl. Phys. Lett. 45 (1984) 284.
- [3] X.-C. Zhang, Y. Jin, X.F. Ma, Appl. Phys. Lett. 61 (1992) 2764.
- [4] A. Rice, Y. Jin, X.F. Ma, et al., Appl. Phys. Lett. 64 (1994) 1324.
- [5] Q. Wu, X.-C. Zhang, Appl. Phys. Lett. 67 (1995) 3523.
- [6] P.U. Jepsen, C. Winnewisser, M. Schall, et al., Phys. Rev. E53 (1996) 3052.
- [7] A. Nahata, A.S. Weling, T.F. Heinz, Appl. Phys. Lett. 69 (1996) 2321.
- [8] Q. Wu, X.-C. Zhang, Appl. Phys. Lett. 70 (1997) 1784.
- [9] C. Winnewisser, P.U. Jepsen, M. Schall, et al., Appl. Phys. Lett. 70 (1997) 3069.
- [10] P.C.M. Planken, H.-K. Nienhuys, H.J. Bakker, et al., J. Opt. Soc., Am. B 18 (2001) 313.
- [11] P.Y. Han, X.-C. Zhang, Meas. Sci. Technol. 12 (2001) 1747.
- [12] M.C. Beard, G.M. Turner, C.A. Schmuttenmaer, J. Phys. Chem. B 106 (2002) 7146.
- [13] C.A. Schmuttenmaer, Chem. Rev. 104 (2004) 1759.
- [14] J.J. Carey, J. Zawadzka, D.A. Jaroszynski, et al., Phys. Rev. Lett. 84 (2000) 1431.
- [15] J. Pearce, Z. Jian, D.M. Mittleman, Phys. Rev. Lett. 91 (2003) 043903.
- [16] H. Cao, A. Nahata, Opt. Express 12 (2004) 1004.
- [17] J. Saxler, J.G. Rivas, C. Janke, et al., Phys. Rev. B 69 (2004) 155427.

- [18] S.P. Jamison, J. Shen, D.R. Jones, et al., *J. Appl. Phys.* 93 (2003) 4334.
- [19] H.-T. Chen, R. Kersting, G.C. Cho, *Appl. Phys. Lett.* 83 (2003) 3009.
- [20] I. Wilke, A.M. MacLeod, W.A. Gillespie, et al., *Phys. Rev. Lett.* 88 (2002) 124801.
- [21] G. Berden, S.P. Jamison, A.M. MacLeod, et al., *Phys. Rev. Lett.* 93 (2004) 114802.
- [22] A. Nahata, D.H. Auston, C. Wu, et al., *Appl. Phys. Lett.* 67 (1995) 1358.
- [23] H.J. Bakker, G.C. Cho, H. Kurz, et al., *J. Opt. Soc., Am. B* 15 (1998) 1795.
- [24] A. Leitenstorfer, S. Hunsche, J. Shah, et al., *Appl. Phys. Lett.* 74 (1999) 1516.
- [25] G. Gallot, D. Grischkowsky, *J. Opt. Soc., Am. B* 16 (1999) 1204.
- [26] J. Faure, J.v. Tilborg, R.A. Kaindl, et al., *Opt. Quantum Electron.* 36 (2004) 681.
- [27] B.I. Greene, J.F. Federici, D.R. Dykaar, et al., *Appl. Phys. Lett.* 59 (1991) 893.
- [28] J.J. Carey, R.T. Bailey, D. Pugh, et al., *Appl. Phys. Lett.* 81 (2002) 4335.
- [29] M.L. Groot, M.H. Vos, I. Schlichting, et al., *Proc. Natl. Acad. Sci. USA* 99 (2002) 1323.
- [30] M.C. Beard, G.M. Turner, C.A. Schmuttenmaer, *J. Phys. Chem. A* 106 (2002) 878.
- [31] J. Xu, A.B. Stickrath, P. Bhattacharya, et al., *Biophys. J.* 85 (2003) 1128.
- [32] G.I. Groma, A. Colonna, J.-C. Lambry, et al., *Proc. Natl. Acad. Sci. USA* 101 (2004) 7971.
- [33] A. Leitenstorfer, S. Hunsche, J. Shah, et al., *Phys. Rev. B* 61 (2000) 16642.
- [34] E. Hendry, M. Koeberg, J.M. Schins, et al., *Phys. Rev. B* 70 (2004) 033202.
- [35] E. Beaurepaire, G.M. Turner, S.M. Harrel, et al., *Appl. Phys. Lett.* 84 (2004) 3465.
- [36] Y.R. Shen, *The Principles of Nonlinear Optics*, Wiley, New York, 1986.
- [37] J. Ahn, A.V. Efimov, R.D. Averitt, et al., *Opt. Express* 11 (2003) 2486.
- [38] K. Wynne, R.M. Hochstrasser, *Adv. Chem. Phys.* 107 (1999) 263.
- [39] C.J.F. Böttcher, *Theory of Electric Polarization*, Elsevier, Amsterdam, 1973.
- [40] C.-P. Hsu, X. Song, R.A. Marcus, *J. Phys. Chem. B* 101 (1997) 2546.
- [41] P.U. Jepsen, R.H. Jacobson, S.R. Keiding, *J. Opt. Soc., Am. B* 13 (1996) 2424.
- [42] M. Born, E. Wolf, *Principles of Optics*, Pergamon Press, Oxford, 1993.
- [43] J.J. Carey, D. Jones, S.P. Jamison, et al., Presented at the Ultrafast Phenomena XIII, Vancouver, Canada, 2002 (unpublished).
- [44] E.D. Palik (Ed.), *Handbook of Optical Constants of Solids*, Academic Press, Orlando, 1985.
- [45] E. Åkesson, A.E. Johnson, N.E. Levinger, et al., *J. Chem. Phys.* 96 (1992) 7859.
- [46] S.A. Kovalenko, N. Eilers-Koenig, T.A. Senyushkina, et al., *J. Phys. Chem. A* 105 (2001) 4834.
- [47] G. Haran, W.D. Sun, K. Wynne, et al., *Chem. Phys. Lett.* 274 (1997) 365.
- [48] M.C. Beard, C.A. Schmuttenmaer, *J. Chem. Phys.* 114 (2001) 2903.
- [49] D.A. Jaroszynski, B. Ersfeld, G. Giraud, et al., *Nucl. Instrum. Meth. A* 445 (2000) 317.
- [50] G.A. Seber, C.J. Wild, *Nonlinear Regression*, Wiley, New York, 1989.
- [51] G. Gallot, J. Zhang, R.W. McGowan, et al., *Appl. Phys. Lett.* 74 (1999) 3450.
- [52] M. Schall, M. Walther, P.U. Jepsen, *Phys. Rev. B* 64 (2001) 094301.
- [53] R.E. Nahory, H.Y. Fan, *Phys. Rev.* 156 (1967) 825.
- [54] M. Schall, H. Helm, S.R. Keiding, *Int. J. Infrared Millimeter Waves* 20 (1999) 595.
- [55] B.N. Flanders, R.A. Cheville, D. Grischkowsky, et al., *J. Phys. Chem.* 100 (1996) 11824.